Macromolecules

pubs.acs.org/Macromolecules Article

Designing Cooperative Hydrogen Bonding in Polyethers with Carboxylic Acid Pendants

Geehwan Kwon,[▽] Minseong Kim,[▽] Woo Hyuk Jung,[▽] Suebin Park, Thi-Thanh Huynh Tam, Seung-Hwan Oh, Soo-Hyung Choi, Dong June Ahn,* Sang-Ho Lee,* and Byeong-Su Kim*

Cite This: *Macromolecules* 2021, 54, 8478–8487 Read Online

ACCESS | Metrics & More | Article Recommendations | Supporting Information

ABSTRACT: As a primary molecular interaction governing unique phenomena found in nature, hydrogen bonding (H-bonding) has played a significant role in the design of functional polymeric materials. We herein present the design and synthesis of poly(glycidoxy acetic acid) (PGA), which involved H-bonding donor and acceptor moieties within a single repeating unit of polyether for the precise control of the cooperative H-bonding in polymer chains. The monomer-activated ring-opening polymerization of a functional epoxide monomer, *t*-butyl glycidoxy acetate, followed by hydrolysis, produced the desired PGA polymers in a controlled manner. The high-level synergistic interplay between the intermolecular and intramolecular H-bonding in the PGA chains was demonstrated with pH-dependent self-association properties in the solution state and stronger adhesion properties in the bulk state compared with the conventional H-bonding mixture of poly(ethylene oxide) and poly(acrylic acid). Furthermore, the molecular dynamics simulations reveal the relative contributions of the respective H-bonding interactions within the polymers in both the solution and the bulk states, thereby highlighting their crucial role in the properties of PGA. Finally, we anticipate the potential applicability of PGA in biological and biomedical fields due to its excellent biocompatibility.

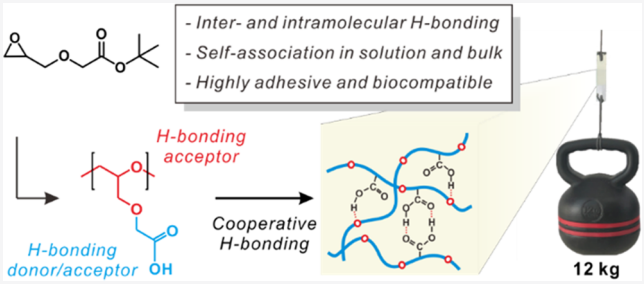

INTRODUCTION

As a primary molecular interaction governing unique phenomena found in nature, including DNA and protein, hydrogen (H)-bonding provides a key for their functionality in inheritance and peptide expression. For example, an array of precisely placed multiple H-bonding allows for strong and specific interactions between complementary base pairs to form the double helix structure in DNA.[1] Furthermore, H-bonding plays a crucial role in the secondary structures of polypeptides, where the α-helix conformation can be stabilized by intramolecular H-bonding, whereas the β-sheet conformation is stabilized by intermolecular H-bonding for unique structures and functions of proteins.[2−5]

Inspired by this weak yet cooperative H-bonding interaction, significant advances have been made in the design and synthesis of novel functional polymers and materials, especially self-assembled supramolecules, polymer blends, copolymers, and nanocomposites.[6,7] Specifically, H-bonding has several profound effects on the physical, chemical, thermal, and mechanical properties of polymers and their assemblies.[8] As a representative example, Meijer et al. introduced strong multiple H-bonding moieties such as benzene-1,3,5-tricarboxamide into polymer chains, affecting the supramolecular folding behavior of the latter to induce proteinlike high-order architectures.[9] Meanwhile, Hawker et al. reported how blends of block copolymers with H-bonding sites in the same block segments lead to highly ordered microphase separation.[10]

Unlike these examples based on the utilization of a specific array of H-bonding chemical motifs, there are also active investigations into exploiting the H-bonding between chains of different polymers to create interpolymer complexes and blends. Within this context, Pipe et al. achieved high thermal conductivity by blending two homopolymers with high miscibility using interchain H-bonding interactions.[11] Furthermore, nanoscale thin films can be assembled using layer-by-layer assembly on the basis of H-bonding. Since the first demonstration by the Rubner group and further exploration by both the Sukhishvili and the Hammond groups, it has been demonstrated that H-bonded interpolymer thin-film complexes can form multilayers between the H-bond donor and acceptor that can also undergo pH-responsive degradation.[12−14] Meanwhile, the integration of poly(ethylene oxide) (PEO) and poly(acrylic acid) (PAA) has particularly received considerable

Received: June 18, 2021
Published: September 13, 2021

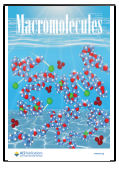

https://doi.org/10.1021/acs.macromol.1c01314
Macromolecules 2021, 54, 8478–8487

Scheme 1. Representative Synthetic Scheme for the Preparation of (a) *t*-Butyl Glycidoxy Acetate (*t*-BGA) Monomer and (b) Monomer-Activated Ring-Opening Polymerization (MAROP) of the P(*t*-BGA) and the Subsequent Acidic Hydrolysis for the Preparation of the Poly(glycidoxy acetic acid) (PGA) (See the Experimental Section for Details)

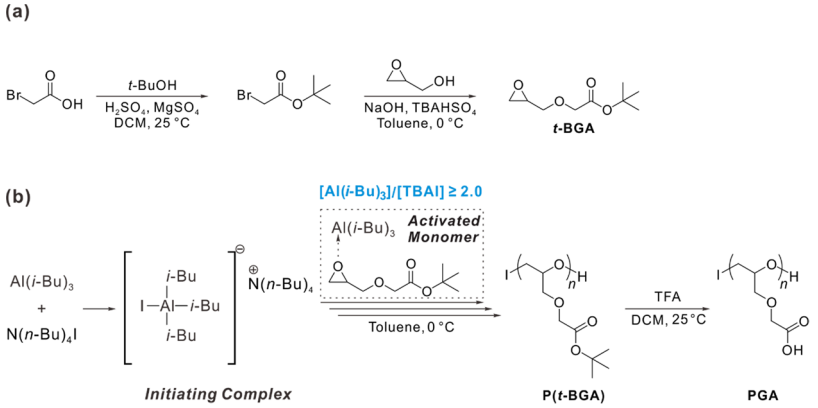

attention in the generation of elastomeric flexible film and surface-based drug delivery platforms.[14−20]

Despite the successful tuning of polymer properties via the intermolecular H-bonding between polymer chains, we envision that the structural designs can be further improved by inducing dynamic interactions between the intermolecular and intramolecular H-bonds in the polymer chains. To realize the uniform and homogeneous distribution of H-bonds throughout a polymer matrix, the H-bond donor and acceptor moieties must be not only homogeneously dispersed but also miscible at a molecular level to allow the polymer chains to intertwine within the radius of gyration. Precise control of the intermolecular and intramolecular H-bonding in both bulk and solution states is thus expected to lead to more versatile applications with improved chemical and physical properties.

To meet the aforementioned requirements, we herein propose a novel molecular design of polymers that possess both H-bonding donor and acceptor moieties within a single monomer unit, thereby allowing for a high-level control of both the intermolecular and intramolecular H-bonding in the polymer chains. Specifically, poly(glycidoxy acetic acid) (PGA) bearing pendant carboxylic acid groups was synthesized using polyether as a platform, with the desired PGA polymer prepared using a functional epoxide monomer, *t*-butyl glycidoxy acetate (*t*-BGA), using monomer-activated ring-opening polymerization (MAROP) in a controlled manner with narrow dispersity (Scheme 1). Subsequent acidic deprotection allowed for the preparation of the PGA, which exhibited pH-dependent self-association in solution and bulk adhesion through the interplay of the intermolecular and intramolecular H-bonding. Importantly, the relative contribution of the respective H-bonding types within the polymer chains was further confirmed by performing molecular dynamics (MD) simulations with reference to the mixture of PEO and PAA homopolymers. Finally, we anticipate the potential applications of PGA in biological and biomedical fields due to its excellent biocompatibility.

EXPERIMENTAL SECTION

Material and Reagents. Bromoacetic acid (Sigma-Aldrich; >97%), *t*-butyl alcohol (Alfa Aesar; >99%), magnesium sulfate (Duksan, EP grade), glycidol (Sigma-Aldrich; >96%), triisobutylaluminum (Al(*i*-Bu)$_3$) solution (1.0 M in hexane; Sigma-Aldrich), tetrabutylammonium iodide (TBAI; Sigma-Aldrich; >98%), trifluoroacetic acid (TFA; Tokyo Chemical Industry; >99%), copper(I) bromide (Sigma-Aldrich, 99.99% trace metals basis), and sulfuric acid (Samchun, 95%) were used as received. Toluene was dried, degassed using a solvent purification system (Vacuum Atmospheres), and collected for immediate use. The monomer *t*-butylacrylate (Sigma-Aldrich, 98%) was passed through a plug of basic alumina to remove the inhibitors prior to use, whereas *N*,*N*,*N*′,*N*″,*N*″-pentamethyldiethylenetriamine (PMDETA; Sigma-Aldrich, 99%) and *t*-butyl *α*-bromoisobutyrate (Sigma-Aldrich, >98%) were bubbled using dry argon for more than 15 min immediately before use. Deuterated chloroform ($CDCl_3$), toluene-d_8, deuterated methanol (MeOD), and deuterium oxide (D_2O) were purchased from Cambridge Isotope Laboratories.

Synthesis of *t*-Butyl Glycidoxy Acetate (*t*-BGA). A *t*-BGA monomer was synthesized in two steps by following a previously reported method with slight modifications.[21,22] Tetrabutylammonium hydrogen sulfate ($TBAHSO_4$) (1.75 g, 5.00 mmol) and *t*-butyl bromoacetate (7.28 mL, 50 mmol) were completely dissolved in 50 mL of 40% aqueous NaOH and 50 mL of toluene at 0 °C. Afterward, glycidol (13.91 mL, 200.00 mmol) was added slowly to the mixture at 0 °C, and the subsequent reaction was allowed to proceed for 1 h at the same temperature while monitoring its progress via thin-layer chromatography. The mixture was diluted with water and extracted using ethyl acetate (EtOAc), with the organic layers then washed with brine, dried over $MgSO_4$, and evaporated to afford a crude liquid. The residue was then purified using column chromatography (Hexane/EtOAc, 2/1 v/v) and subsequently vacuum-distilled to leave the desired product as a colorless oil (5.83 g, 62%). ^{1}H NMR (400 MHz, $CDCl_3$) δ 3.97−4.11 (m, 2H), 3.87 (dd, J = 11.5, 3.0 Hz, 1H), 3.50 (dd, J = 11.5, 5.9 Hz, 1H), 3.16−3.24 (m, 1H), 2.81 (dd, J = 4.9, 4.2 Hz, 1H), 2.63 (dd, J = 5.0, 2.7 Hz, 1H), 1.48 (s, 9H). ^{13}C NMR (101 MHz, $CDCl_3$) δ 169.61, 134.02, 133.96, 117.96, 81.57, 72.25, 67.69, 28.12, 28.09. Electrospray ionization mass spectrometry (ESI-MS) (m/z): $[M + Na]^+$ calcd for $C_9H_{16}O_4Na$, 211.09; obs. 211.09.

General Monomer-Activated Ring-Opening Polymerization of the *t*-BGA Monomer. The polymerization was conducted by applying the Schlenk technique under argon in flame-dried glass tubes. A representative synthetic protocol is described as follows. Using a glovebox, TBAI (75.4 mg, 0.20 mmol) was placed in a Schlenk flask before *t*-BGA and toluene were added, and the mixture was cooled down to 0 °C. Subsequently, 5.0 equiv of 1.0 M Al(*i*-Bu)$_3$ solution (1.0 mL, 1.0 mmol) was introduced to the flask to initiate the polymerization. The reaction was monitored via ^{1}H NMR to determine the residual epoxide signals and the conversion of the reaction. When the polymerization was completed after 3 h, an excess amount of methanol was added to terminate the polymerization. After evaporating off the solvent, the mixture was dissolved in methanol and precipitated in distilled water to remove any residual salts. The polymer solution was concentrated in vacuo to obtain P(*t*-BGA) (2.96 g, 79%). ^{1}H NMR (400 MHz, $CDCl_3$) δ 3.97 (s, 2H), 3.74−

https://doi.org/10.1021/acs.macromol.1c01314
Macromolecules 2021, 54, 8478−8487

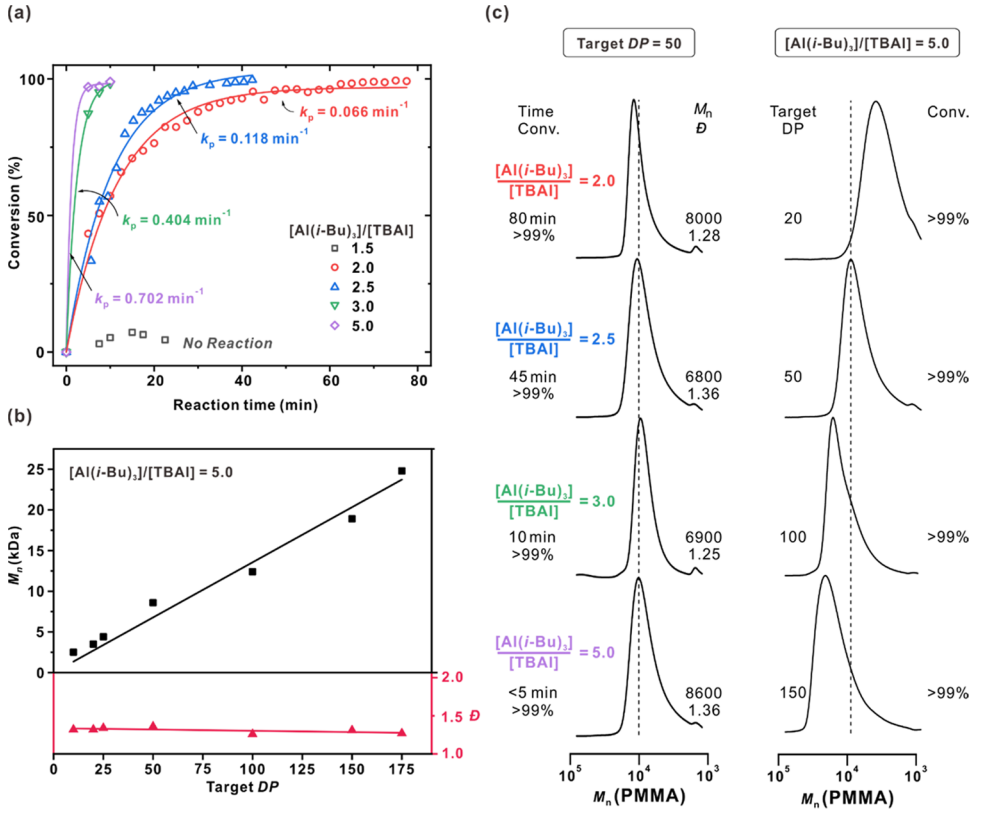

Figure 1. (a) *In situ* ^{1}H NMR kinetics of the polymerization of P(*t*-BGA) by controlling the ratio of [Al(*i*-Bu)$_3$]/[TBAI]. (b) Changes in molecular weight (M_n) and dispersity ($Đ$) during the polymerization of P(*t*-BGA) with varying ratios of [*t*-BGA]/[TBAI] and at a fixed ratio of [Al(*i*-Bu)$_3$]/[TBAI]. (c) Corresponding SEC traces of the respective polymerizations with (left) varying ratios of [Al(*i*-Bu)$_3$]/[TBAI] with a fixed target DP of 50 and (right) varying the target DP with a fixed ratio of [Al(*i*-Bu)$_3$]/[TBAI]. The dotted lines are included to aid the visual comparison. Reaction conditions: [*t*-BGA]$_0$ = 1.0 M in toluene at 0 °C.

3.47 (m, 5H), 1.45 (s, 9H); ^{13}C NMR (101 MHz, $CDCl_3$) δ 169.74, 81.33, 71.62, 69.34, 28.28.

***In Situ* ^{1}H NMR Polymerization Kinetics.** A mixture of TBAI (1.0 equiv) and *t*-BGA monomer (50 equiv) in toluene-d_8 (1.0 M to the monomer) was transferred using a syringe to a conventional NMR tube sealed with a rubber septum before the sample was cooled at 0 °C. Following this, 1.5−5.0 equiv of Al(*i*-Bu)$_3$ was added to the NMR tube, which was then shaken to homogenize the mixture before it was placed in the NMR spectrometer. The sample temperature was set to 0 °C, and spectra were recorded every 2 min (total of 16 scans in 3 h). The integrals of the methylene protons of the monomer (δ = 2.87 ppm for *t*-BGA) were monitored to calculate the monomer consumption with reference to the residual signal of toluene (δ = 2.09 ppm).

Deprotection of Poly(*t*-BGA) to PGA. The deprotection of the P(*t*-BGA) was performed following a previously reported method.[23] A solution of P(*t*-BGA) (2.0 g, 10.6 mmol) in dichloromethane was added to the TFA (4.87 mL, 63.6 mmol) solution in 50 mL of dichloromethane and stirred at 25 °C. After 72 h, the deprotection of the *t*-butyl group was analyzed via ^{1}H NMR, and where necessary, the reaction was continued for a further 24 h under identical conditions to achieve a yield of over 99%. Any solvent and residual TFA were removed in vacuo, and the residual solid was dissolved in methanol and purified via precipitation in ice-cold diethyl ether to obtain the deprotected polymer, PGA. ^{1}H NMR (400 MHz, D_2O) δ 4.25 (s, 2H), 3.63−3.83 (m, 5H); ^{13}C NMR (101 MHz, CD_3OD) δ 177.52, 79.28, 72.08, 71.51, 69.91.

Synthesis of PAA. Polymerization was conducted using the syringe technique under dry argon in baked glass tubes equipped with a three-way stopcock. Here, CuBr (97.5 mg, 0.68 mmol), *t*-butylacrylate (9.96 mL, 6.8 mmol), *t*-butyl α-bromoisobutyrate (0.115 mL, 6.18 mmol), and PMDETA (0.14 mL, 0.68 mmol) were sequentially added to a 50 mL flask filled with argon. Immediately after mixing, the polymerization mixture was placed in an oil bath and maintained at 50 °C for 4 h before the polymerization reaction was terminated by cooling down to −78 °C. The quenched solutions were then evaporated and dissolved in tetrahydrofuran (THF). Any residual catalyst was removed by passing the mixture through silica gel and evaporated off to obtain the products, which were subsequently dried overnight under vacuum at room temperature ($DP_{n,NMR}$ = 100, M_n = 13 800, M_w/M_n = 1.28). Next, 1.0 g of the obtained polymer was dissolved in 10 mL of neat TFA and stirred overnight at room temperature. After removing the TFA under reduced pressure, the crude material was dissolved in THF and precipitated in hexane to obtain PAA as a white solid at a quantitative yield. ^{1}H NMR (300 MHz, D_2O) δ 2.55−2.40 (d, 76 H), 2.06−1.49 (m, 152 H), 1.14 (t, J = 6.9 Hz, 6 H).

pH-Dependent Self-Association in an Aqueous Solution. PGA was dispersed in deionized water at a concentration of 10 mg mL^{-1} with the addition of 1.0 M NaOH solution for full dissolution in water. Then, the 1.0 M HCl was added dropwise to the solution while monitoring changes in transmittance at 500 nm as a function of pH using a UV−vis spectrophotometer.

Lap Shear Adhesion Testing. A 10 μL of the PGA solution in methanol (concentration 100 mg mL^{-1}) was added dropwise on the surface of the specimens before the two specimens were firmly bonded to the 25 × 5 mm^2 surface and then fixed with a binder clip. The sample was then dried in a vacuum oven at 40 °C for 12 h before being cooled down to room temperature prior to the measurements using a universal testing machine (UTM; WL2100C, Withlab). Lap shear adhesion testing was performed with a speed of 1.3 mm min^{-1} and a temperature of 25 °C, with the results reported as the average value of at least three repetitions with the standard deviation. The

https://doi.org/10.1021/acs.macromol.1c01314
Macromolecules 2021, 54, 8478−8487

specimens used were glass, Teflon, poly(methyl methacrylate) (PMMA), polycarbonate (PC), and stainless steel.

RESULTS AND DISCUSSION

Design of a Functional Epoxide Monomer for the MAROP. A glycidyl ether-based functional monomer, *t*-butyl glycidoxy acetate (*t*-BGA), was prepared via a facile two-step reaction starting with bromoacetic acid and *t*-butanol under acidic conditions, followed by a substitution reaction with glycidol (Scheme 1a). The synthesized *t*-BGA monomer was purified via column chromatography and fractional distillation to obtain an isolated yield of 62%. The chemical structure of the *t*-BGA was successfully confirmed using various NMR spectroscopic techniques, including ^{1}H, ^{13}C, correlation spectroscopy (COSY), heteronuclear single-quantum correlation (HSQC), and electrospray ionization mass spectrometry (ESI-MS) (Figure 2 and Figures S1−S4 in the Supporting Information).

The prepared *t*-BGA monomer was then subjected to the monomer-activated ring-opening polymerization (MAROP) using an initiating complex of triisobutylaluminum (Al(*i*-Bu)$_3$) as a catalyst and tetrabutylammonium iodide (TBAI, N(*n*-Bu)$_4$I) as an initiator to yield the P(*t*-BGA). This Lewis acid-catalyzed polymerization enables versatile access to a diverse array of polyethers with sensitive functional moieties.[24−27] By contrast, our initial attempt using conventional anionic ring-opening polymerization with an organic superbase, *t*-BuP$_4$, was unsuccessful due to the potential side reaction in which the benzyl alkoxide initiator reacted with the *t*-butyl ester of the *t*-BGA monomer via nucleophilic substitution and/or elimination (Figure S5).

According to previous literature, it is widely known that there exists an optimum ratio of catalyst to initiator, [Al(*i*-Bu)$_3$]/[TBAI], during MAROP.[24,25,28] In such a case, the Lewis acid Al(*i*-Bu)$_3$ could interact with the *t*-BGA monomer at two possible types of coordinating sites: the oxygen atom in the epoxide ring (CH_2OCH-) and those in the pendant group (ether $-CH_2OCH_2-$ and ester $-CH_2CO_2-$).[25]

We thus performed polymerization of the *t*-BGA monomer with varying ratios of [Al(*i*-Bu)$_3$]/[TBAI] from 1 to 10 while monitoring the conversion of the monomers via *in situ* ^{1}H NMR spectroscopy (Figures 1a, S6, S7, and Table S1). The linear correlation between $\ln([M]_0/[M]_t)$ and the reaction time supported the successful living characteristics of the polymerization of *t*-BGA while varying the [Al(*i*-Bu)$_3$]/[TBAI] ratio (Figure S8). Interestingly, from a ratio of 2.0 upward, the polymerization of *t*-BGA was observed with an increasing propagation constant (k_p) and relatively controlled polymers with narrow dispersity ($Đ$), whereas the reaction rate was almost negligible at the ratios of 1.0 and 1.5 (Figure 1 and Table S1). This was likely due to the trapping of the aluminum catalyst by the oxygen atoms on the pendant group of the *t*-BGA. Hence, the ratio of [Al(*i*-Bu)$_3$]/[TBAI] should be higher than 1.5 to trigger polymerization.[25] As such, we chose the [Al(*i*-Bu)$_3$]/[TBAI] ratio of 5.0 for the polymerization in this study since it would afford a fast reaction with controlled molecular weight dispersity ($Đ$). As shown in Figure 1b, the molecular weight ($M_{n,SEC}$) of the P(*t*-BGA) obtained via SEC analysis increased linearly with the increase in the monomer-to-initiator ratio, [*t*-BGA]/[TBAI], suggesting the controlled growth of the polymers (Figure S9). It was revealed that more than 99% of monomer conversion was observed for P(*t*-BGA) homopolymers of various molecular weights from 2500 to 24 800 g mol^{-1} within 6 h with a unimodal curve with a narrow $Đ$ value within 1.3, as confirmed via SEC analysis (entries 1−7 in Table 1). However, a conversion of only 86% was observed for the polymerization with a target DP of 200, albeit with sufficient polymerization time (entry 8 in Table 1).[26,28]

Table 1. Characterization of the P(*t*-BGA) Polymers Prepared at 5.0 equiv of [Al(*i*-Bu)$_3$]/[TBAI]

entry	DP_{target}	time (h)	conv[a] (%)	$M_{n,theo}$ (g mol^{-1})	$M_{n,SEC}$[b] (g mol^{-1})	$Đ$[b]
1	10	6	>99	2000	2500	1.32
2	20	6	>99	3900	3500	1.32
3	25	6	>99	4800	4400	1.34
4	50	6	>99	9500	8600	1.36
5	100	6	>99	19 000	12 400	1.26
6	150	6	>99	28 400	18 900	1.31
7	175	6	>99	33 100	24 800	1.27
8	200	18	90	37 800	26 000	1.39

[a]Measured via ^{1}H NMR spectroscopy in $CDCl_3$. [b]Measured via size-exclusion chromatography (SEC) calibrated with PMMA standards in DMF (24 mM LiCl, 40 °C, flow rate 1.0 mL min^{-1}).

Structural Analysis of the Polymers. The synthesized P(*t*-BGA)$_{100}$ polymers were characterized via a series of ^{1}H NMR, SEC, and Fourier transform infrared (FT-IR) spectroscopy analyses. As shown in Figure 2, the ^{1}H NMR spectra

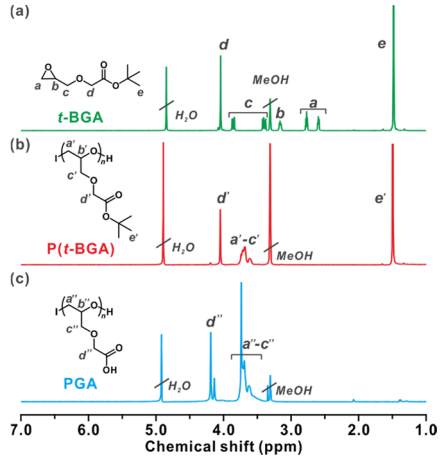

Figure 2. ^{1}H NMR spectra of (a) *t*-BGA monomer, (b) P(*t*-BGA)$_{100}$ (entry 5 in Table 1), and (c) the deprotected PGA$_{100}$. All spectra were collected in CD_3OD solvent.

indicated that the conversion of the monomer into the polymer was accompanied by the disappearance of the epoxide peaks, *a* and *b*, in the monomer at 2.62, 2.81, and 3.20 ppm upon polymerization. Moreover, the other peaks in the P(*t*-BGA)$_{100}$ polymer could be clearly assigned, including those for the polyether backbone protons (3.40−3.75 ppm), methylene protons (*d*′; 4.75−4.85 ppm), and *t*-butyl protons (*e*′; 1.46 ppm). Subsequently, deprotection of the P(*t*-BGA) was followed by treatment with trifluoroacetic acid (TFA) to produce the desired PGA polymer in a high yield, typically over 98%. It was found that the characteristic *t*-butyl protons observed at 1.46 ppm disappeared following the deprotection, with the deprotection confirmed via ^{13}C NMR (Figures S10 and S11). Note that the calculation of the $M_{n,NMR}$ based on the end group analysis was limited because of the absence of a

https://doi.org/10.1021/acs.macromol.1c01314
Macromolecules 2021, 54, 8478−8487

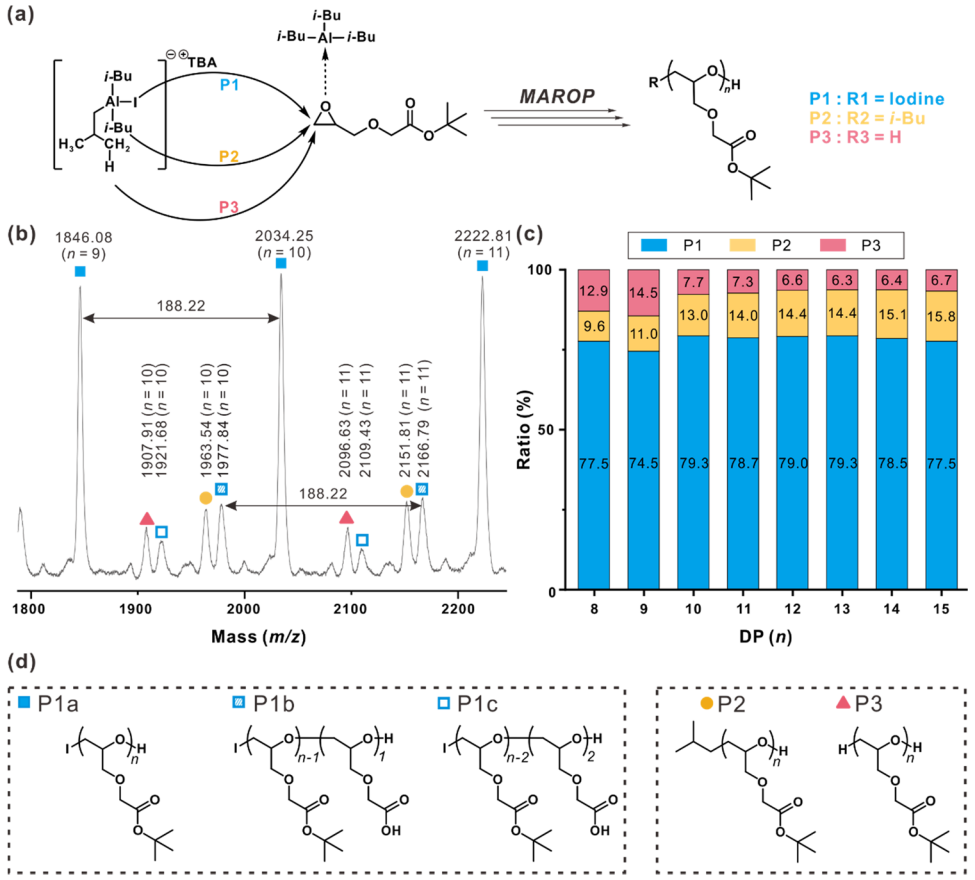

Figure 3. (a) Analysis of potential side reactions occurring in the initiation step of the MAROP. (b) Representative MALDI-ToF spectrum of P(*t*-BGA)$_{10}$ (entry 1 in Table 1) in the *m*/*z* range of 1800−2300 Da with individual peak assignments. (c) Analyzed distribution histogram of respective initiating groups in the synthesized P(*t*-BGA) polymers and (d) the corresponding chemical structures of polymers (P1−P3) with varying initiating groups. Note that the partially degraded polymeric fragments (P1b and P1c) were observed during the measurement.

characteristic peak resulting from using iodine as the initiator. In all cases, functional moieties were clearly observed via FT-IR analysis. For example, the disappearance of the characteristic epoxide peak at 904 cm^{-1} and the *t*-butyl peak at 1368 cm^{-1} revealed the polymerization along with deprotection to afford the desired PGA polymer (Figure S12).

Encouraged by the successful polymerization of the *t*-BGA monomer using MAROP, we further explored the mechanistic details by analyzing the initiation steps using matrix-assisted laser desorption/ionization-time of flight (MALDI-ToF) analysis (Figures 3 and S13). As demonstrated in previous reports, the MALDI-ToF was employed for evaluation of the absolute molecular weight and end group analysis as well as the polymer topologies, which provides a convenient means to assess the relative contents of polymers with different initiating species.[29,30] It is known that the initiation step can involve hydrogen or the *t*-butyl group from Al(*i*-Bu)$_3$ besides the desired iodine group, as shown in Figure 3a.[31,32] As a representative example, P(*t*-BGA)$_{10}$ (entry 1 in Table 1) was selected to determine the degree of initiation from each group. It can be observed that the majority of the peaks originated from the initiation of iodine; for example, the observed *m*/*z* of 2034.25 can be assigned to a homopolymer comprised of the iodine initiator (126.90) and 10 monomers (188.22), with Na^+ as the counterion (Figure 3b). Additionally, the relatively small fractions of peaks originated from the initiation by the hydrogen or *t*-butyl groups (P2 and P3 in Figure 3c). Most importantly, the spacing of the major and minor signals corresponded to the molecular weight of the functional *t*-BGA monomer, thus indicating the successful polymerization. Based on the molecular weight calculations in the collected MALDI-ToF spectrum, it was clear that approximately 80% of the P(*t*-BGA) resulted from the initiation with iodine, as shown in Figure 3c. This relatively high contribution of the initiation group is important when considering the fidelity of the conjugation with other chemical moieties to the prepared polymers. Moreover, it is interesting to note that there were two types of minor peaks resulting from the partial degradation of the *t*-butyl group during the measurement (P1b and P1c in Figure 3d).

The glass transition temperature (T_g) of the representative polymers was obtained via thermal analysis using differential scanning calorimetry (DSC). For example, the P(*t*-BGA)$_{100}$ exhibited a T_g of −17.4 °C, which increased significantly to 10 °C upon deprotection due to the H-bonding in the PGA polymer chains (Figure S14). According to the Fox equation, a T_g of 14 °C was estimated on the basis of the equimolar mixture of PEO (T_g of −76.6 °C) and PAA (T_g of 101 °C). Similarly, Frey and co-workers recently reported the T_g of ester-functionalized polyethers, including methyl 4,5-epoxypentenoate and *t*-butyl 4,5-epoxypentenoate, to be 41 and −25 °C, respectively.[33]

Self-Association in the Aqueous PGA Solution. An aqueous solution of PGA retained a highly negative charge with a ζ-potential value of −44.3 mV at pH 7 because of the deprotonation of all of the carboxylic acids in the pendant

https://doi.org/10.1021/acs.macromol.1c01314
Macromolecules 2021, 54, 8478−8487

groups of the PGA under neutral conditions (Figure S15). As the degree of protonation increased upon addition of the 1.0 M HCl solution, the transmittance tended to decrease from approximately pH 3 before dropping sharply to 0% at pH 2.5 (Figure 4). Considering the pK_a of a typical polymeric carboxylic acid is in the range of 4.7−5.0, it is possible to state that this behavior occurs via the intermolecular H-bonds present in the PGA, including the carboxylic acid in the side chain, with the oxygen atoms in the polyether backbone acting in accordance with the carboxylic acid dimers in the side chains of other polymers.[34] In addition, the action of these H-bonds can be further corroborated by their contribution to the intramolecular interactions in PGA. The presence of intermolecular and intramolecular H-bonding was confirmed by increasing the solution temperature of the PGA under different pH conditions (i.e., pH 1 and pH 3) while monitoring the transmittance of the solution. It was found that the transmittance increased gradually even at the pH 1 condition, suggesting that the observed transmittance changes originated from the dynamic H-bonding (Figure S16). It was also interesting to observe that the transmittance from the PGA increased slightly because of the formation of an insoluble precipitate under highly acidic conditions (pH 1).

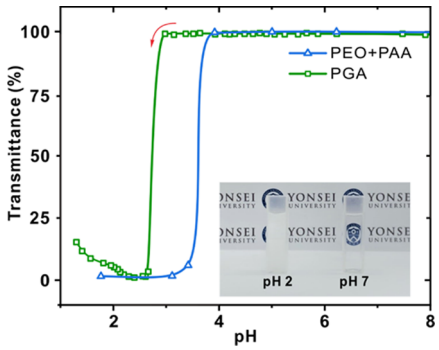

Figure 4. Changes in the transmittance at 500 nm of the aqueous PGA_{100} solution (green) and the mixture of PEO_{100} and PAA_{100} solution (blue) under varying pH conditions. The concentration of the polymers was set to 10 mg mL^{-1}. The inset image corresponds to the PGA solution at pH 2 and pH 7.

For comparison, we performed control experiments with a solution mixture of PEO (H-bond acceptor) and PAA (H-bond donor), in which interpolymer H-bonding complexes are known to form under acidic conditions well below the pK_a value of PAA (i.e., typically below pH 3).[14] Here, we set the DP of each polymer to 100 to eliminate any possible factors associated with molecular weights. In addition, we fixed the concentration of each solution to be identical to that of PGA to elucidate the critical role of H-bonding in the context of inter- and intrapolymer complex formation in the solution. Although the PEO or PAA alone did not exhibit any sign of transmittance change with the decrease in pH (Figure S17),

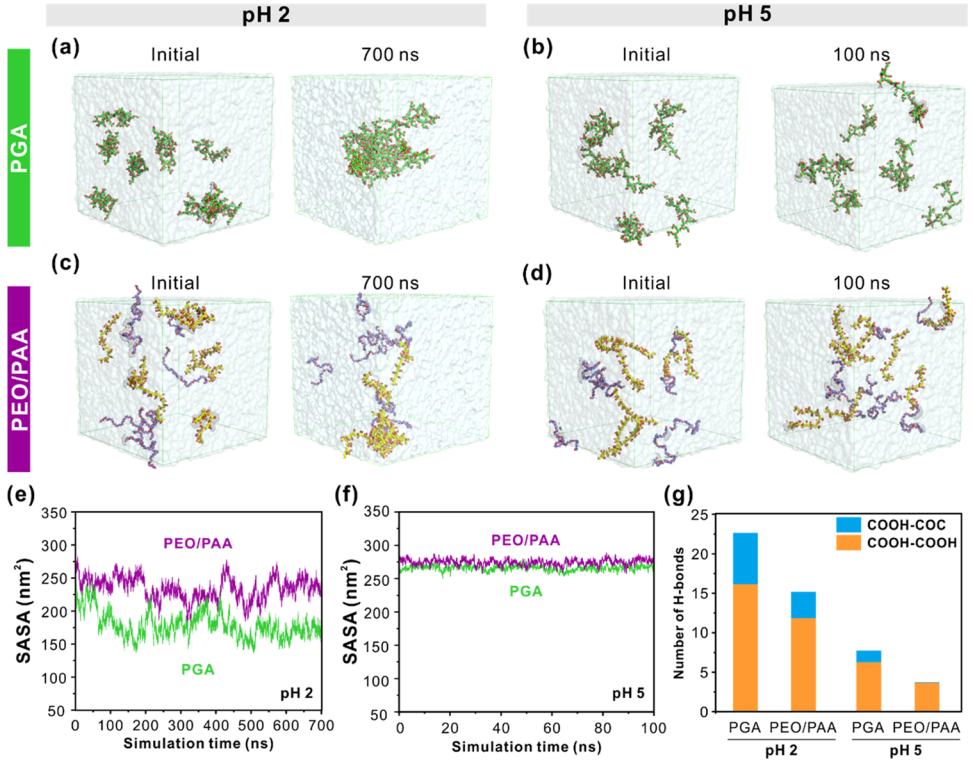

Figure 5. All-atom molecular dynamics (MD) simulations of self-association of the aqueous solution of the PGA and the PEO/PAA mixture at pH 2 and pH 5. Initial and final configurations of the PGA solution at (a) pH 2 and (b) pH 5. The carbon, oxygen, and hydrogen atoms in the PGA are displayed in green, red, and white, respectively, whereas the water molecules are shown as a transparent cyan surface for clarity. Initial and final configurations of the PEO/PAA mixture solution at (c) pH 2 and (d) pH 5. The carbon atoms of PEO and PAA are displayed in yellow and purple, respectively. (e, f) Time-lapsed solvent-accessible surface area (SASA) of the PGA and PEO/PAA solution at (e) pH 2 and (f) pH 5. (g) Comparison of the number of H-bonds in the final configurations of the aqueous solution of the PGA and PEO/PAA mixture at pH 2 and pH 5. (Blue) COOH−COC indicates the H-bonds between carboxylic acid groups and the polyether backbone, and (orange) COOH−COOH designates H-bonds between the carboxylic acids.

https://doi.org/10.1021/acs.macromol.1c01314
Macromolecules 2021, 54, 8478−8487

Table 2. Summary of the Intermolecular and Intramolecular H-Bonding of the PGA and the PEO/PAA Mixture under Different Conditions Using MD Simulations

		intermolecular		intramolecular		
polymer	condition	COOH−COOH[a]	COOH−COC[b]	COOH−COOH[a]	COOH−COC[b]	total
PGA	solution (pH 2)	11.57 ± 3.76	5.28 ± 1.60	4.56 ± 2.24	1.28 ± 1.12	22.69
	solution (pH 5)	0.066 ± 0.29	0.005 ± 0.077	6.16 ± 2.55	1.44 ± 1.20	7.73
	bulk	449.2 ± 7.2	159.6 ± 6	110.4 ± 4.4	54.8 ± 3.2	774
PEO/PAA	solution (pH 2)	10.56 ± 3.84	3.36 ± 1.84	1.28 ± 1.20	ND	15.19
	solution (pH 5)	0	0.082 ± 0.28	3.68 ± 1.44	ND	3.76
	bulk	418 ± 5.6	289.6 ± 6.8	46 ± 2.4	ND	753.6

[a]H-bonding interaction among the carboxylic acid groups. [b]H-bonding interaction between the carboxylic acid and the polyether backbone.

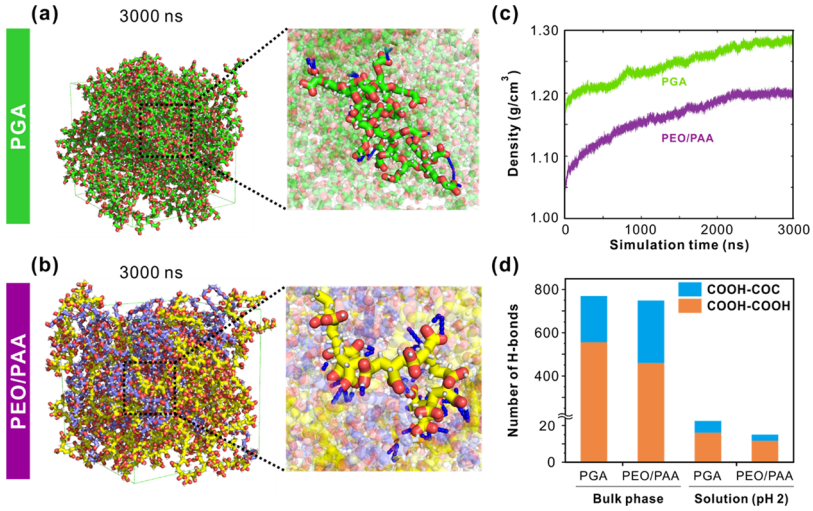

Figure 6. Final configurations of the molecular dynamics (MD) simulations for the (a) PGA and (b) PEO/PA and the corresponding H-bonding networks in the PGA and the PEO/PAA mixture. (c) Time-dependent density variation of polymers in the bulk state. (d) Comparison of the number of H-bonds in the final configurations of the PGA and the PEO/PAA mixture in the bulk and solution states at pH 2. (Blue) COOH−COC indicates the H-bonding between the carboxylic acid groups and the polyether backbone, and (orange) COOH−COOH denotes the H-bonding among the carboxylic acid groups.

the solution mixture demonstrated a drastic transmittance change similar to that observed with the PGA solution owing to the H-bonding, which confirmed that PGA retains both its polyether backbone and the carboxylic acid pendant groups that are responsible for the dynamic H-bonding. It is also worth noting that the onset of the transmittance decrease occurred earlier at a relatively higher pH for the solution mixture of PEO/PAA than with the PGA, suggesting that the pK_a value of PGA is lower than that of PAA, which can be attributed to the presence of the adjacent polyether backbone facilitating the deprotonation of the carboxylic acid pendant groups. For example, the pH value determined at a transmittance change of nearly 50% corresponded to pH 2.77 for the PGA and 3.61 for the PEO/PAA. The observed critical pH corresponded well with the values reported for layer-by-layer assembled thin films of PEO/PAA at pH 3.6, where the H-bonded layers disintegrated upon deprotonation of the PAA segments.[18]

All-Atom MD Simulations for Self-Association. To elucidate the difference between the self-association of PGA and PEO/PAA at a molecular level, we conducted all-atom molecular dynamics (MD) simulations of systems containing eight polymer chains of PGA and PEO/PAA at pH 2 (all protonated) (Figure 5). In the system constructed using PGA, all of the polymers became organized into a larger cluster by the end of the 700 ns simulation (Figure 5a). Meanwhile, although a large cluster was also formed in the system with the PEO/PAA mixture, some polymer chains remained unassociated until the end of the simulation (Figure 5c). We then performed simulations of the PGA and PEO/PAA solutions at pH 5 to verify the effect of pH on the self-association process (Figure 5b,d). In this case, half of the carboxylic acid moieties were assumed to be deprotonated based on the pK_a values. In both systems, no cluster formation was observed following the 100 ns simulation due to the repulsion of the negative charges between the carboxylic acid groups, suggesting the crucial role of the latter in forming the H-bonding network in association with the polymeric chains.

To compare the aggregation propensity between the systems with PGA and PEO/PAA in a quantitative manner, the solvent-accessible surface area (SASA) was calculated (Figure 5e,f). Here, the SASA of the PGA decreased from approximately 240−170 nm^2 (ca. 71%), whereas that of the PEO/PAA mixture decreased from approximately 260−230 nm^2 (ca. 88%) at pH 2. These results again indicate that the self-association in PGA is more pronounced than that in a PEO/PAA mixture. Unlike the result observed at pH 2, with a pH of 5, the SASA value fluctuated at around 260 and 280 nm^2 for the PGA and the PEO/PAA mixture, respectively, indicating that the self-association process does not occur at pH 5. Moreover, the number of H-bonds formed in the polymers that lead to self-association was determined (Figure

https://doi.org/10.1021/acs.macromol.1c01314
Macromolecules 2021, 54, 8478−8487

5g), with the number of H-bonds formed at pH 2 found to be 22.69 for the PGA and 15.19 for the PEO/PAA, which were significantly higher than those found at pH 5 (7.73 for the PGA and 3.76 for the PEO/PAA) (Table 2). Taken together from the simulation results, we propose that the stronger H-bonding networks formed in the PGA at pH 2 induced the self-association process, which is in good agreement with the experimental results.

To further investigate the association behavior of PGA and PEO/PAA in the bulk state, amorphous polymeric systems containing 40 polymer chains of both PGA and PEO/PAA were constructed under fully protonated conditions. The density of the polymers in the bulk state was monitored throughout the simulation to confirm the equilibration of the systems (Figure 6a,c). For both systems, the density of the polymers increased slowly before reaching a plateau at around 2.3 μs. The density of the PGA (1.29 g cm^{-3}) was approximately 8.4% higher than that of the PEO/PAA mixture (1.19 g cm^{-3}) at 3.0 μs (Figure 6b). Following the equilibration, detailed analyses indicated that the number of H-bonds formed in the PGA and PEO/PAA systems in the bulk state was 774 and 753.6, respectively, which exceeded those in the solution state by nearly eightfold for each polymer chain (Figure 6d). Furthermore, it was noted that the number of H-bonds was comparatively higher in the PGA systems in both the solution and the bulk state, which was in line with the higher aggregation propensity of PGA due to the contribution from intramolecular H-bonding. Table 2 summarizes the information collected via the MD simulations.

Encouraged by the significantly high contribution of the intramolecular and intermolecular H-bonds in the PGA system, as demonstrated through the MD simulation, we performed a rheological measurement of the PGA polymer. Specifically, the temperature-dependent viscoelastic properties of the PGA$_{100}$ were characterized within the range of 20−130 °C (Figure S18). It is remarkable that the G' was larger than the G'' at a 1% strain and 1 rad s^{-1} frequency over the measured temperature range, suggesting that the PGA$_{100}$ behaved like a solid up to 130 °C, although mainly weakly entangled chains were expected. Note that the entanglement molecular weight of PEO is 1600 g mol^{-1} (DP ∼ 37).[35] Additionally, compared with the zero-shear viscosity (η) of polyether-based polymers without H-bonding motifs,[36] the PGA$_{100}$ exhibited a considerably high complex viscosity (η^*) of at least 5 orders of magnitude at room temperature. Thus, it is clear that the interchain interaction of H-bonding significantly hinders the chain dynamics of PGA.

Adhesive Properties of PGA Polymers. Since their reversible nature makes H-bonded materials particularly attractive to create synthetic adhesive materials,[37,38] we set out to assess the potential of the PGA in relation to adhesives. Specifically, lap shear tests were performed using a UTM to evaluate the effects of the H-bonding in polymer chains on the adhesive properties (Figure 7a). First, the optimal loading amount of PGA for the adhesive strength was evaluated using varying amounts of PGA solution in methanol (from 0.08 to 4.0 mg cm^{-2}), which were loaded on the glass substrates and dried in a vacuum oven at 40 °C. The optimal adhesion of PGA$_{100}$ was observed at 0.16 mg cm^{-2} for glass substrates with a shear stress of 1.34 MPa (Figures 7c and S19a). Unlike with the PGA$_{100}$ sample, the adhesion strength of the PEO/PAA mixture with an identical DP as the PGA$_{100}$ did not clearly depend on the loading amount of polymer mixture in the range

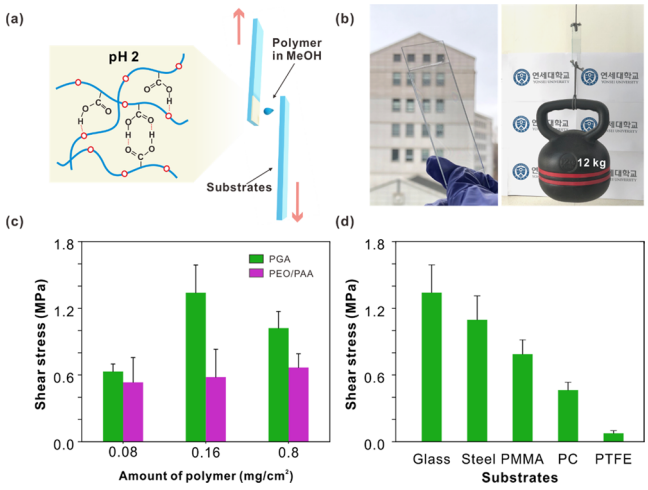

Figure 7. Lap shear adhesion testing of the PGA and PEO/PAA mixture samples. (a) Schematic representation of the PGA polymer coating on the substrates. (b) Photographs of the PGA-coated glass substrate (left) and lift-up of a 12 kg dumbbell using the PGA-coated glass substrate (right). (c) Shear stress of the polymer samples with respect to the amount of polymer samples. (d) Shear stress of the PGA polymer with various substrates. A PGA$_{100}$ sample of 0.16 mg cm^{-2} was used.

of 0.08−0.8 mg cm^{-2} (Figure 7c). This observation likely originated from the more homogeneous H-bonding between PGA polymer chains compared with that in the PEO/PAA mixture. By taking advantage of the optimum adhesion of PGA$_{100}$, the lift-up of a 12 kg dumbbell was performed using the PGA-coated glass substrate. It is also interesting to note that the PGA$_{100}$ adhesive was highly transparent on visual inspection (Figure 7b).

Moreover, the optimal polymer chain length for effective H-bonding between the polymer chains was determined using PGA$_{50}$, PGA$_{100}$, and PGA$_{150}$ at a fixed polymer amount of 0.16 mg cm^{-2}. Interestingly, the PGA$_{100}$ displayed the optimal adhesion among all of the samples (Figure S19b), albeit with a constant ratio between the H-bonding donor and acceptor. Here, the different polymer chain lengths may have affected the self-association behavior via the intermolecular and intramolecular H-bonding based on the different conformational changes. As such, the adhesive properties were further expanded to other substrates, including steel, PMMA, PC, and PTFE, with the substrates carrying more H-bonding sites and the PGA polymer found to demonstrate a stronger adhesion performance (Figure 7d). The detailed characterization of the adhesive properties of PGA in terms of different compositions and structures will be the subject of our future research efforts.

Finally, the biocompatibility of the PGA polymers was evaluated using the 3-(4,5-dimethylthiazol-2-yl)-2,5-diphenyltetrazolium bromide (MTT) assay toward the human cervical cancer cells (HeLa) as a model cell line. Here, the PGA$_{100}$ exhibited a superior cellular viability of approximately 100% up to a high concentration of 1000 μg mL^{-1}, posing its high potential for biological and biomedical applications (Figure S20).

■ CONCLUSIONS

In summary, we report the design and synthesis of PGA, which consists of H-bonding donor and acceptor moieties within a single repeating unit of polyether. By applying a MAROP of

https://doi.org/10.1021/acs.macromol.1c01314
Macromolecules 2021, 54, 8478−8487

the novel functional epoxide monomer *t*-BGA, followed by acidic deprotection, the desired PGA was obtained in a highly controlled manner with narrow dispersity. A highly cooperative H-bonding between the intermolecular and intramolecular H-bonding at the PGA polymer chains was demonstrated with pH-dependent self-association properties in the solution, as well as strong bulk adhesion compared with the conventional H-bonding assembly mixture of PEO and PAA. Furthermore, the MD simulations revealed the relative contributions of the respective H-bonding within the polymers, both in the solution and in the bulk state, highlighting the critical role of the cooperative H-bonding interactions in PGA. We anticipate that the new class of functional epoxide monomer and the polymers developed in this study will contribute to the development of functional polyethers, posing high potential in biological and biomedical applications.

■ ASSOCIATED CONTENT

Supporting Information

The Supporting Information is available free of charge at https://pubs.acs.org/doi/10.1021/acs.macromol.1c01314.

NMR, ESI-MS, FT-IR, MALDI-ToF, polymerization kinetics, DSC, rheology analysis, lap shear test, and MTT assay of PGA_{100} polymer (PDF)

■ AUTHOR INFORMATION

Corresponding Authors

Dong June Ahn − *Department of Chemical and Biological Engineering and KU-KIST Graduate School of Converging Science and Technology, Korea University, Seoul 02841, Republic of Korea;* orcid.org/0000-0001-5205-9168; Email: ahn@korea.ac.kr

Sang-Ho Lee − *Center for Advanced Specialty Chemicals, Korea Research Institute of Chemical Technology, Ulsan 44412, Republic of Korea;* orcid.org/0000-0003-2207-3369; Email: slee@krict.re.kr

Byeong-Su Kim − *Department of Chemistry, Yonsei University, Seoul 03722, Republic of Korea;* orcid.org/0000-0002-6419-3054; Email: bskim19@yonsei.ac.kr

Authors

Geehwan Kwon − *Department of Chemistry, Yonsei University, Seoul 03722, Republic of Korea*

Minseong Kim − *Department of Chemistry, Yonsei University, Seoul 03722, Republic of Korea; Department of Chemistry, Ulsan National Institute of Science and Technology (UNIST), Ulsan 44919, Republic of Korea;* orcid.org/0000-0002-2612-922X

Woo Hyuk Jung − *Department of Chemical and Biological Engineering, Korea University, Seoul 02841, Republic of Korea;* orcid.org/0000-0001-5169-4223

Suebin Park − *Department of Chemistry, Yonsei University, Seoul 03722, Republic of Korea*

Thi-Thanh Huynh Tam − *Center for Advanced Specialty Chemicals, Korea Research Institute of Chemical Technology, Ulsan 44412, Republic of Korea*

Seung-Hwan Oh − *Department of Chemical Engineering, Hongik University, Seoul 04066, Republic of Korea*

Soo-Hyung Choi − *Department of Chemical Engineering, Hongik University, Seoul 04066, Republic of Korea;* orcid.org/0000-0002-4078-6285

Complete contact information is available at: https://pubs.acs.org/10.1021/acs.macromol.1c01314

Author Contributions

[▽]G.K., M.K., and W.H.J. contributed equally to this work.

Notes

The authors declare no competing financial interest.

■ ACKNOWLEDGMENTS

This work was also supported by Samsung Research Funding & Incubation Center of Samsung Electronics under Project Number SRFC-MA1602-07.

■ REFERENCES

(1) Watson, J. D.; Crick, F. H. C. Molecular Structure of Nucleic Acids: A Structure for Deoxyribose Nucleic Acid. *Nature* **1953**, *171*, 737−738.

(2) Pauling, L.; Corey, R. B.; Branson, H. R. The Structure of Proteins: Two Hydrogen-Bonded Helical Configurations of the Polypeptide Chain. *Proc. Natl. Acad. Sci. U.S.A.* **1951**, *37*, 205−211.

(3) Hofman, A. H.; van Hees, I. A.; Yang, J.; Kamperman, M. Bioinspired Underwater Adhesives by Using the Supramolecular Toolbox. *Adv. Mater.* **2018**, *30*, No. 1704640.

(4) Jin, J.; Hassanzadeh, P.; Perotto, G.; Sun, W.; Brenckle, M. A.; Kaplan, D.; Omenetto, F. G.; Rolandi, M. A Biomimetic Composite from Solution Self-Assembly of Chitin Nanofibers in a Silk Fibroin Matrix. *Adv. Mater.* **2013**, *25*, 4482−4487.

(5) Wang, J.; Zhang, D.; Chu, F. Wood-Derived Functional Polymeric Materials. *Adv. Mater.* **2020**, *33*, No. 2001135.

(6) Qing, G.; Lu, Q.; Li, X.; Liu, J.; Ye, M.; Liang, X.; Sun, T. Hydrogen Bond Based Smart Polymer for Highly Selective and Tunable Capture of Multiply Phosphorylated Peptides. *Nat. Commun.* **2017**, *8*, No. 461.

(7) Cheng, C. C.; Wang, J. H.; Chuang, W. T.; Liao, Z. S.; Huang, J. J.; Huang, S. Y.; Fan, W. L.; Lee, D. J. Dynamic Supramolecular Self-Assembly Hydrogen Bonding-Induced Contraction and Extension of Functional Polymers. *Polym. Chem.* **2017**, *8*, 3294−3299.

(8) Guo, M.; Pitet, L. M.; Wyss, H. M.; Vos, M.; Dankers, P. Y. W.; Meijer, E. W. Tough Stimuli-Responsive Supramolecular Hydrogels with Hydrogen-Bonding Network Junctions. *J. Am. Chem. Soc.* **2014**, *136*, 6969−6977.

(9) Ter Huurne, G. M.; Voets, I. K.; Palmans, A. R. A.; Meijer, E. W. Effect of Intra- versus Intermolecular Cross-Linking on the Supramolecular Folding of a Polymer Chain. *Macromolecules* **2018**, *51*, 8853−8861.

(10) Tang, C.; Lennon, E. M.; Fredrickson, G. H.; Kramer, E. J. Hawker, C. J. Evolution of Block Copolymer Lithography to Highly Ordered Square Arrays. *Science* **2008**, *322*, 429−432.

(11) Kim, G. H.; Lee, D.; Shanker, A.; Shao, L.; Kwon, M. S.; Gidley, D.; Kim, J.; Pipe, K. P. High Thermal Conductivity in Amorphous Polymer Blends by Engineered Interchain Interactions. *Nat. Mater.* **2015**, *14*, 295−300.

(12) Cheung, J. H.; Stockton, W. B.; Rubner, M. F. Molecular-Level Processing of Conjugated Polymers. 3. Layer-by-Layer Manipulation of Polyaniline via Electrostatic Interactions. *Macromolecules* **1997**, *30*, 2712−2716.

(13) Gallivan, J. P.; Dougherty, D. A. A Computational Study of Cation-π Interactions vs Salt Bridges in Aqueous Media: Implications for Protein Engineering. *J. Am. Chem. Soc.* **2000**, *122*, 870−874.

(14) Lutkenhaus, J. L.; Hrabak, K. D.; McEnnis, K.; Hammond, P. T. Elastomeric Flexible Free-Standing Hydrogen-Bonded Nanoscale Assemblies. *J. Am. Chem. Soc.* **2005**, *127*, 17228−17234.

(15) Anderson, E. R.; Daga, V. K.; Gido, S. P.; Watkins, J. J. Hydrogen Bond Mediated Self-Assembly of Two Diblock Copolymers. *J. Polym. Sci.* **2020**, *58*, 3061−3068.

(16) Chen, Y. W.; Yeh, B. J.; Hashimoto, T.; Liao, S. Y.; Lo, C. T. Hydrogen Bonding Induced Co-Ordering and Interfacial Curvature

Controlled Crystallization Behavior of Binary Copolymer Blends. *Macromolecules* **2018**, *51*, 7699−7712.
(17) Xiang, F.; Ward, S. M.; Givens, T. M.; Grunlan, J. C. Structural Tailoring of Hydrogen-Bonded Poly(Acrylic Acid)/Poly(Ethylene Oxide) Multilayer Thin Films for Reduced Gas Permeability. *Soft Matter* **2015**, *11*, 1001−1007.
(18) Sukhishvili, S. A.; Granick, S. Layered, Erasable Polymer Multilayers Formed by Hydrogen-Bonded Sequential Self-Assembly. *Macromolecules* **2002**, *35*, 301−310.
(19) Kim, B. S.; Park, S. W.; Hammond, P. T. Hydrogen-Bonding Layer-by-Layer-Assembled Biodegradable Polymeric Micelles as Drug Delivery Vehicles from Surfaces. *ACS Nano* **2008**, *2*, 386−392.
(20) Kim, B. S.; Lee, H.; Il; Min, Y.; Poon, Z.; Hammond, P. T. Hydrogen-Bonded Multilayer of pH-Responsive Polymeric Micelles with Tannic Acid for Surface Drug Delivery. *Chem. Commun.* **2009**, *28*, 4194−4196.
(21) Wright, S. W.; Hageman, D. L.; Wright, A. S.; McClure, L. D. Convenient Preparations of *t*-Butyl Esters and Ethers from *t*-Butanol. *Tetrahedron Lett* **1997**, *38*, 7345−7348.
(22) Tian, Z.; Menard, F. Synthesis of Kainoids and C4 Derivatives. *J. Org. Chem.* **2018**, *83*, 6162−6170.
(23) Filippov, A. D.; Van Hees, I. A.; Fokkink, R.; Voets, I. K.; Kamperman, M. Rapid and Quantitative De-*tert*-Butylation for Poly(Acrylic Acid) Block Copolymers and Influence on Relaxation of Thermoassociated Transient Networks. *Macromolecules* **2018**, *51*, 8316−8323.
(24) Gervais, M.; Brocas, A. L.; Cendejas, G.; Deffieux, A.; Carlotti, S. Synthesis of Linear High Molar Mass Glycidol-Based Polymers by Monomer-Activated Anionic Polymerization. *Macromolecules* **2010**, *43*, 1778−1784.
(25) Roos, K.; Dolci, E.; Carlotti, S.; Caillol, S. Activated Anionic Ring-Opening Polymerization for the Synthesis of Reversibly Cross-Linkable Poly(Propylene Oxide) Based on Furan/Maleimide Chemistry. *Polym. Chem.* **2016**, *7*, 1612−1622.
(26) Gervais, M.; Brocas, A. L.; Deffieux, A.; Ibarboure, E.; Carlotti, S. Rapid and Controlled Synthesis of Hydrophobic Polyethers by Monomer Activation. *Pure Appl. Chem.* **2012**, *84*, 2103−2111.
(27) Labbé, A.; Carlotti, S.; Billouard, C.; Desbois, P.; Deffieux, A. Controlled High-Speed Anionic Polymerization of Propylene Oxide Initiated by Onium Salts in the Presence of Triisobutylaluminum. *Macromolecules* **2007**, *40*, 7842−7847.
(28) Brocas, A.; Cendejas, G.; Caillol, S.; Deffieux, A. Stephane Carlotti. Controlled Synthesis of Polyepichlorohydrin with Pendant Cyclic Carbonate Functions for Isocyanate-Free Polyurethane Networks. *J. Polym. Sci., Part A: Polym. Chem.* **2011**, *49*, 7207−7224.
(29) Liu, J.; Loewe, R. S.; McCullough, R. D. Employing MALDI-MS on Poly(Alkylthiophenes): Analysis of Molecular Weights, Molecular Weight Distributions, End-Group Structures, and End-Group Modifications. *Macromolecules* **1999**, *32*, 5777−5785.
(30) Asenjo-Sanz, I.; Veloso, A.; Miranda, J. I.; Pomposo, J. A.; Barroso-Bujans, F. Zwitterionic Polymerization of Glycidyl Monomers to Cyclic Polyethers with $B(C_6F_5)_3$. *Polym. Chem.* **2014**, *5*, 6905−6908.
(31) Sakakibara, K.; Nakano, K.; Nozaki, K. Regioregular Polymerization of Fluorine-Containing Epoxides. *Macromolecules* **2007**, *40*, 6136−6142.
(32) Sakakibara, K.; Nakano, K.; Nozaki, K. Regio-Controlled Ring-Opening Polymerization of Perfluoroalkyl-Substituted Epoxides. *Chem. Commun.* **2006**, *31*, 3334−3336.
(33) Linker, O.; Blankenburg, J.; Maciol, K.; Bros, M.; Frey, H. Ester Functional Epoxide Monomers for Random and Gradient Poly(Ethylene Glycol) Polyelectrolytes with Multiple Carboxylic Acid Moieties. *Macromolecules* **2020**, *53*, 3524−3534.
(34) Michaels, A. S.; Morelos, O. Polyelectrolyte Adsorption by Kaolinite. *Ind. Eng. Chem.* **1955**, *47*, 1801−1809.
(35) Fetters, L. J.; Lohse, D. J.; Richter, D.; Witten, T. A.; Zirkel, A. Connection between Polymer Molecular Weight, Density, Chain Dimensions, and Melt Viscoelastic Properties. *Macromolecules* **1994**, *27*, 4639−4647.
(36) Jung, H.; Gang, S. E.; Kim, J. M.; Heo, T. Y.; Lee, S.; Shin, E.; Kim, B. S.; Choi, S. H. Regulating Dynamics of Polyether-Based Triblock Copolymer Hydrogels by End-Block Hydrophobicity. *Macromolecules* **2020**, *53*, 10339−10348.
(37) Mazzotta, M. G.; Putnam, A. A.; North, M. A.; Wilker, J. J. Weak Bonds in a Biomimetic Adhesive Enhance Toughness and Performance. *J. Am. Chem. Soc.* **2020**, *142*, 4762−4768.
(38) Li, X.; Lai, J.; Deng, Y.; Song, J.; Zhao, G.; Dong, S. Supramolecular Adhesion at Extremely Low Temperatures: A Combined Experimental and Theoretical Investigation. *J. Am. Chem. Soc.* **2020**, *142*, 21522−21529.

https://doi.org/10.1021/acs.macromol.1c01314
Macromolecules 2021, 54, 8478−8487